DOI: 10.1002/anie.201307290

Imaging agents

Cell Tracking with Caged Xenon: Using Cryptophanes as MRI Reporters upon Cellular Internalization**

*Stefan Klippel, Jörg Döpfert, Jabadurai Jayapaul, Martin Kunth, Federica Rossella, Matthias Schnurr, Christopher Witte, Christian Freund, and Leif Schröder**

Abstract: *Caged xenon has great potential in overcoming sensitivity limitations for solution-state NMR detection of dilute molecules. However, no application of such a system as a magnetic resonance imaging (MRI) contrast agent has yet been performed with live cells. We demonstrate MRI localization of cells labeled with caged xenon in a packed-bed bioreactor working under perfusion with hyperpolarized-xenon-saturated medium. Xenon hosts enable NMR/MRI experiments with switchable contrast and selectivity for cell-associated versus unbound cages. We present MR images with 10^3-fold sensitivity enhancement for cell-internalized, dual-mode (fluorescence/MRI) xenon hosts at low micromolar concentrations. Our results illustrate the capability of functionalized xenon to act as a highly sensitive cell tracer for MRI detection even without signal averaging. The method will bridge the challenging gap for translation to in vivo studies for the optimization of targeted biosensors and their multiplexing applications.*

Conventional MRI contrast agents for cell labeling that are based on changes in proton spin relaxivity often suffer from limited differentiation between unspecific background signals and labeled areas.[1] In vivo detection of such agents at low concentrations is challenging, whereas toxicity must be considered as the labeling efficiency increases.[2,3] One method to overcome the background problem is "hot spot" MRI,[4] as shown for applications with ^{19}F-based cell trackers. Measurements are however characterized by a relatively low signal-to-noise ratio (SNR), owing to the restricted ^{19}F spin densities achieved by common labeling approaches.[5] Additional limitations arise when aiming for the detection of sensors with different NMR signals, or sensors that can change their signal upon binding or upon a biochemical reaction. Several techniques were proposed that address the sensitivity limitation using hyperpolarized nuclei.[6]

Xenon-129 is inert, making it particularly suitable as a candidate for biomedical applications.[7] Hyperpolarization increases its detectable magnetization by 4–5 orders of magnitude, which allows for in vivo MRI, as demonstrated by various preclinical studies in humans.[8–10] Xenon-MRI can be paired with a targeting approach by reversibly trapping xenon atoms in molecular cages to form so-called biosensors that include a targeting moiety for a particular analyte.[11] Such reversible host–guest complexes also allow for indirect detection through saturation transfer techniques without significantly impairing the relaxation behavior of hyperpolarized xenon (hp-xenon).[12]

Herein, we demonstrate the ability to use lipophilic cryptophanes as xenon hosts for cell-labeling and reporting cellular internalization of caged xenon, which is experiencing very favorable exchange conditions for efficient saturation-transfer-based MRI detection. This provides the first data on the imaging performance of caged xenon in live cellular environments with a 10^6-fold reduced acquisition time.

The receptor-mediated cellular internalization of a xenon biosensor was recently monitored by NMR spectroscopy at high cell density (140 million/sample), high concentration of hp-xenon, and using extensive signal averaging, but without performing MRI experiments.[13] Although sensitivity can be increased by using saturation-transfer methods such as hyper-CEST,[14] other NMR studies reporting the binding of scaffolded biosensors to cell surface receptors[15] did not perform imaging.

We previously demonstrated that the key to efficient use of the hyper-CEST approach for MRI applications is to provide enough xenon magnetization to work with fast encoding schemes and to allow for relatively fast xenon exchange (for example, in nonpolar solvents).[16] As a consequence, the strong signal of free xenon in solution shows sufficient induced depletion to perform the MRI of test solutions with nanomolar concentrations of caged xenon, while maintaining chemical-shift selectivity for different sensors.[16]

The motivation for using lipophilic cryptophane-A monoacid (CrA-ma) for cell tracking is as follows: Partitioning of dye-labeled cryptophane-A cages into artificial biomembranes was recently characterized by combining fluorescence techniques and hyper-CEST spectroscopy.[17] Such data revealed a characteristic NMR frequency shift for caged xenon when embedded into pure lipid membranes, but also

[*] S. Klippel, J. Döpfert, Dr. J. Jayapaul, M. Kunth, F. Rossella, M. Schnurr, Dr. C. Witte, Dr. L. Schröder
ERC Project BiosensorImaging
Leibniz-Institut für Molekulare Pharmakologie (FMP)
13125 Berlin (Germany)
E-mail: lschroeder@fmp-berlin.de
Homepage: https://www.fmp-berlin.de/schroeder
S. Klippel, Dr. C. Freund
Protein Biochemistry Group, Freie Universität Berlin
14195 Berlin (Germany)

[**] This work has been supported by the European Research Council under the European Community's Seventh Framework Programme (FP7/2007-2013)/ERC grant agreement no. 242710, the Leibniz Association (WGL; grant SAW-2011-FMP-2) and the Human Frontier Science Program.

Supporting information for this article, including experimental details, is available on the WWW under http://dx.doi.org/10.1002/anie.201307290.

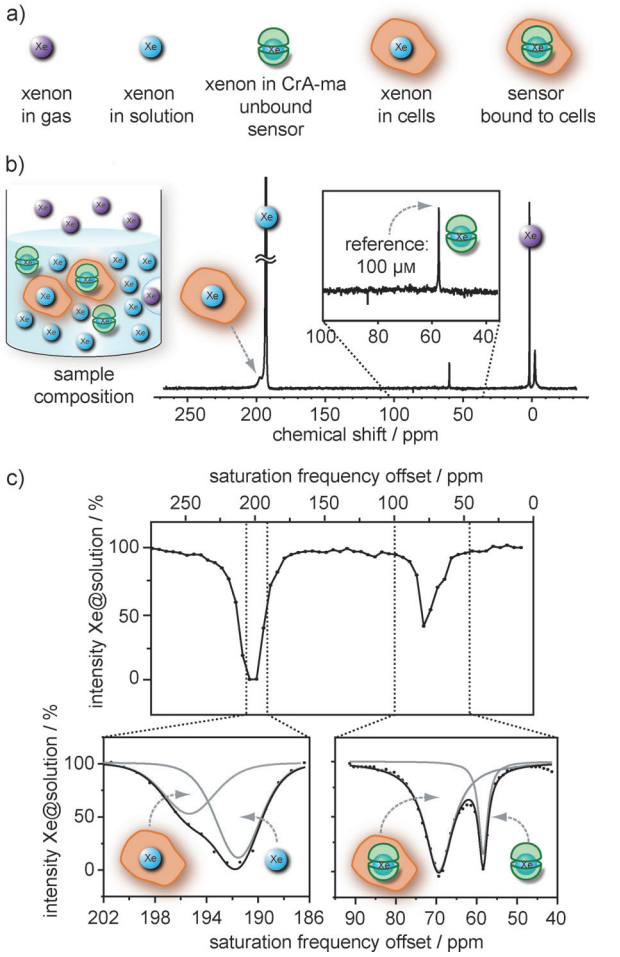

Figure 1. The xenon NMR-signature of CrA-ma labeled cells observed by direct detection and indirect hyper-CEST detection. a) Detected xenon pools. b) The average of 64 direct scans reveals the presence of four different xenon pools, but the signal of xenon caged in cell-bound CrA-ma is missing. c) Hyper-CEST spectroscopy allows the detection of the highly diluted pool of xenon caged in cell-bound CrA-ma at a saturation frequency offset of 69 ppm. The signal is separated from the reference signal of unbound CrA-ma by 11 ppm, allowing for frequency-selective hyper-CEST MRI (Figure S3). Exponential Lorentzian fits are shown as grey lines, and the corresponding sums are shown as black lines.

for lipid mixtures.[18] Similar signals have been observed without CEST amplification for cells incubated with CrA-labeled proteins.[13] Our findings reveal that localization of cryptophane-labeled cells can be achieved, even with a single hyper-CEST acquisition, at low micromolar cage concentrations, thus demonstrating very sensitive MRI cell tracking.

Mouse fibroblasts (L929) were incubated for 3 h with 90 μM CrA-ma dissolved in cell culture medium before they were washed and resuspended at medium density (15 million cells mL^{-1}). To monitor the expected chemical shift of cage-entrapped xenon upon cell association, excess CrA-ma (100 μM) was added to act as a chemical shift reference. Hp-xenon was directly bubbled into the cell suspension, and foam formation was reduced by an antifoaming agent (Supporting Information, Materials and Methods, Figure S1). An accumulation of 64 direct scans reveals four different xenon pools: xenon in solution within cells (Xe@cells: 196 ppm), xenon in solution (Xe@sol: 192 ppm), xenon in free CrA-ma (Xe@CrA-ma: 59 ppm), and xenon in the gas phase (Xe@gas: 0 ppm; Figure 1 a,b). The signal of xenon in cell-associated CrA-ma could not be observed by direct acquisition and was therefore probed by acquiring hyper-CEST spectra. Prior to detecting the abundant signal of free xenon in solution, a selective saturation pulse was swept over the chemical shift range of 250–5 ppm in 5 ppm steps (cw-saturation for 8 s with 6.5 μT). We could observe two asymmetric saturation responses centered around 200 ppm and ca. 70 ppm (Figure 1 c, top). By optimizing the saturation pulse power (186–202 ppm: cw-saturation for 8 s with 2.1 μT) and decreasing the step size of the applied saturation pulses to 1 ppm, each response was revealed to be a superposition of two peaks (Figure 1 c, bottom). Compared to direct readout, an additional resonance could be detected at 69 ppm, which was assigned (Figure S2) to xenon in cell-associated CrA-ma (Xe@CrA-ma@cells). Cell binding of CrA-ma therefore leads to a ca. 10 ppm downfield shift for the entrapped xenon signal at 22 °C. The concentration of cell-bound CrA-ma is much lower than the concentration of unbound CrA-ma, as indicated by the lack of the 69 ppm peak in the direct spectrum (Figure 1 b). Although the CEST response for both cage peaks show comparable intensities, it is likely that once it is cell/membrane-associated, the xenon experiences very favorable exchange conditions, thus improving hyper-CEST detection.

To elucidate the cellular localization and to quantify the intracellular concentration of cryptophane in the attempted hyper-CEST MRI demonstrations, we synthesized a fluorescein-bearing cryptophane conjugate (CrA-FAM; see the

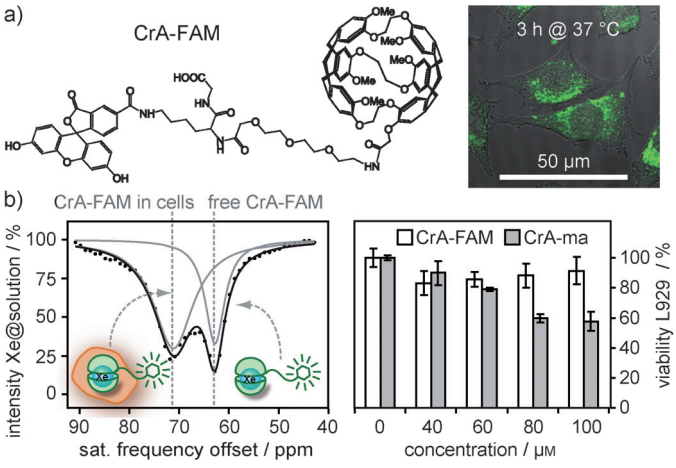

Figure 2. Verification of the MRI performance of cryptophane-labeled cells by coupling the cage to fluorescein through a three-unit PEG-linker. a) The resulting dual mode contrast agent, CrA-FAM (left), allows for quantitative and localized fluorescence experiments in parallel to NMR. CrA-FAM (green) is cell internalized (incubation: 3 h, 75 μM @ 37 °C), as observed by fluorescence microscopy (right; see also Figure S11). b) Hyper-CEST spectroscopy allows CrA-FAM inside and outside cells to be distinguished, based on a 9 ppm frequency difference for caged xenon (left; see also Figure S4). The construct shows reduced toxicity compared to unmodified CrA-ma, exceeding an incubation concentration of 60 μM (incubation: 20 h @ 37 °C, right). Error bars show the standard deviation from eight runs.

Materials and Methods section of the Supporting Information). The construct shows improved water solubility, reduced toxicity, and appears all over the cytoplasm, where it is presumably internalized in membranes of lysosomal vesicles owing to fluid phase pinocytosis, as proposed by Boutin et al. for a BSA-coupled cryptophane molecule (Figure 2; see also Figure S11).[13] The observed hyper-CEST response (cw-saturation for 12 s with 6.5 μT; Xe@CrA-FAM@cells: 71 ppm, Xe@CrA-FAM: 63 ppm) is similar to unmodified CrA-ma at 37 °C (Figure S2), which points to a cellular internalization of both constructs, although for the unmodified CrA-ma this cannot ultimately be proven.

The chemical-shift selectivity of the hyper-CEST technique enables selective MRI of cell internalized cryptophane, even in the presence of unbound cryptophane in solution (for CrA-ma, see Figure S3; for CrA-FAM, see Figure S4). The hyper-CEST intensity for cells labeled with CrA-FAM is 2.5-fold lower than unmodified CrA-ma (Figure S10). Fluorescein coupling reduces the hydrophobicity of the construct, resulting in a decreased uptake by cells.

Xenon delivery by direct bubbling into cell suspensions is problematic because bursting gas bubbles can create strong forces, leading to cell death[15] and fragmentation, as demonstrated by centrifugation experiments (Figure S2). To prevent premature cell death and to simulate in vivo delivery of hp-xenon into immobile tissue structures, we designed an NMR-compatible packed-bed bioreactor working under continuous perfusion with an hp-xenon-saturated medium. The gas is introduced into the culture medium within a bubbling chamber sitting upstream of the sample phantom (Figure S5).[19] The phantom was split into two compartments along the direction of media flow. Cells were immobilized by encapsulating them at medium density (ca. 10 million cells mL^{-1}) within solid alginate beads (ca. 10000 cells/bead; Figure S6).[20] One of the two compartments was filled with cells preincubated for 20 h with 50 μM CrA-FAM after alginate encapsulation. By measuring the fluorescence intensity of cell lysates[21] (see the Materials and Methods section of the Supporting Information) the average intracellular concentration of CrA-FAM was estimated to be ca. 15 μM. This estimation assumes a homogeneous distribution of CrA-FAM over the whole cell volume. The second compartment was filled with beads carrying unlabeled cells (Figure 3a). Figure 3c shows a hyper-CEST image recorded at 37 °C in combination with laser scanning microscopy done both before and after the MRI measurements. The strength of the applied cw-saturation pulse was increased to 18 μT. Because of the continuous flow, unbound CrA-FAM is washed out with the medium making a frequency separation unnecessary. The hyper-CEST effect was calculated based on the average of 20 on-resonant (saturation on Xe@CrA-FAM@cells: 68 ppm) and 20 off-resonant (saturation at 326 ppm) images acquired with a CEST-weighted RARE sequence (see the Materials and Methods section of the Supporting Information).[22,23] The percentage signal reduction for on-resonant saturation was analyzed compared to off-resonant saturation for each pixel (normalized signals with $<30\%$ intensity were ignored; Figure S8). The image (32×32 pixels) was resized by cyclic spline interpolation to the resolution of the underlying proton

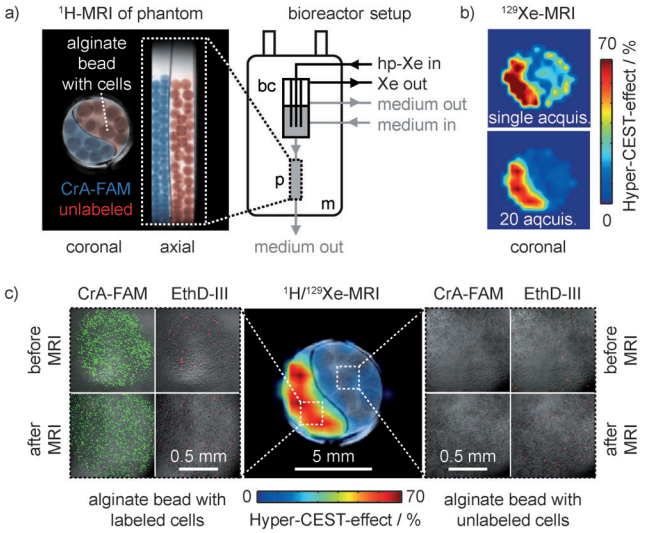

Figure 3. Hyper-CEST-effect of CrA-FAM-labeled cells (intracellular concentration = 15 μM) analyzed within a continuous flow bioreactor. a) Proton-MRI of a two compartment phantom housing cells encapsulated within alginate beads. The compartments were colored using graphic design software for visualization. One compartment is filled with CrA-FAM labeled cells (blue), whereas cells within the second compartment are unlabeled (red). The sample phantom is perfused with hp-xenon saturated medium. bc = bubbling chamber, m = magnet, p = phantom. b) The localization of the compartment bearing ca. two million labeled cells could be achieved in a single CEST-acquisition (2 min) at the expense of a higher noise level compared to the accumulation of 20 CEST-acquisitions. c) Hyper-CEST-effect as a result of 20 on-resonant/off-resonant RARE-images clearly reveals the localization of labeled cells (center). Laser scanning microscopy (optical section of single alginate beads) done before and after MRI shows CrA-FAM (green) accumulation within encapsulated cells. Dead cells are stained with Ethidium homodimer III (red). Live cells in the control compartment do not give a contrast in either MRI or fluorescence scans.

MRI (256×256 pixels). The compartment bearing labeled cells could be clearly distinguished from the control compartment by a CEST effect of up to 70 %, although the localization could also be achieved in single CEST acquisitions at the expense of a higher noise level (Figure 3c). Our approach allows extended hyper-CEST-MRI experiments at physiological temperature while maintaining cell viability at approximately 90 % (Figure 3c).

We have shown that hyper-CEST-MRI is sensitive and selective enough to visualize cell-internalized xenon hosts at low micromolar concentrations, even without signal averaging. The achieved signal amplification in this study can be roughly estimated as follows: The SNR for the cage resonance at 100 μM concentration in Figure 1b is ca. 35 for 64 xenon deliveries. Increasing the temperature to 36 °C reduces the SNR ca. 2.2-fold.[24] Assuming the slice thickness for the single CEST-acquisition images in Figure 3b is not more than that for unlocalized acquisition in Figure 1b, the available xenon signal is spread over ca. 85 pixels for 625 μm in-plane resolution. Despite a ca. 6.7-fold lower concentration (15 μM), higher temperature, and the distribution over 85 pixels, an SNR of ca. 2.5 is achieved after only two xenon deliveries (Figure 3b). Thus, the enhancement is ca. 2700-fold

and allows us to reduce the acquisition time by a factor of 2700^2, that is, ca. 7×10^6.

In summary, aside from the demonstrated possibility of cell tracking after ex situ labeling, caged xenon offers the potential of targeting disease-associated biomarkers in vivo.[13,15,25–27] The method and setup presented here enables the evaluation of the NMR/MRI performance of such xenon-based biosensors in detail. A combination of both optimized in vivo delivery of hp-xenon (which is currently under investigation,[28,29] with conceivable delivery of hp-xenon to any organ in the body[30]) and optimized in vitro characterization of biosensors and MRI read-out schemes, is necessary to bridge the challenging gap for translating the concept to the first animal experiments.

Received: August 19, 2013
Published online: December 4, 2013

Keywords: cell tracking · host-guest systems · hyper-CEST · NMR imaging · xenon

[1] E. T. Ahrens, R. Flores, H. Xu, P. A. Morel, *Nat. Biotechnol.* **2005**, *23*, 983 – 987.
[2] K. A. Sterenczak, M. Meier, S. Glage, M. Meyer, S. Willenbrock, P. Wefstaedt, M. Dorsch, J. Bullerdiek, H. M. Escobar, H. Hedrich, et al., *BMC Cancer* **2012**, *12*, 284.
[3] P. C. Wang, L. Shan, *J. Basic Clin. Med.* **2012**, *1*, 1 – 6.
[4] J. W. M. Bulte, *Nat. Biotechnol.* **2005**, *23*, 945 – 946.
[5] J. Ruiz-Cabello, B. P. Barnett, P. A. Bottomley, J. W. M. Bulte, *NMR Biomed.* **2011**, *24*, 114 – 129.
[6] C. Witte, L. Schröder, *NMR Biomed.* **2013**, *26*, 788 – 802.
[7] L. Schröder, *Phys. Med.* **2013**, *29*, 3 – 16.
[8] J. P. Mugler, T. A. Altes, *J. Magn. Reson. Imaging* **2013**, *37*, 313 – 331.
[9] Y. Shukla, A. Wheatley, M. Kirby, S. Svenningsen, A. Farag, G. E. Santyr, N. A. M. Paterson, D. G. McCormack, G. Parraga, *Acad. Radiol. Acta Radiol.* **2012**, *19*, 941 – 951.
[10] K. Qing, K. Ruppert, Y. Jiang, J. F. Mata, G. W. Miller, Y. M. Shim, C. Wang, I. C. Ruset, F. W. Hersman, T. A. Altes, et al., *J. Magn. Reson. Imaging* **2013**, DOI: 10.1002/jmri.24181.
[11] M. M. Spence, S. M. Rubin, I. E. Dimitrov, E. J. Ruiz, D. E. Wemmer, A. Pines, S. Q. Yao, F. Tian, P. G. Schultz, *Proc. Natl. Acad. Sci. USA* **2001**, *98*, 10654 – 10657.
[12] D. M. L. Lilburn, G. E. Pavlovskaya, T. Meersmann, *J. Magn. Reson.* **2013**, *229*, 173 – 186.
[13] C. Boutin, A. Stopin, F. Lenda, T. Brotin, J.-P. Dutasta, N. Jamin, A. Sanson, Y. Boulard, F. Leteurtre, G. Huber, et al., *Bioorg. Med. Chem.* **2011**, *19*, 4135 – 4143.
[14] L. Schröder, T. J. Lowery, C. Hilty, D. E. Wemmer, A. Pines, *Science* **2006**, *314*, 446 – 449.
[15] K. K. Palaniappan, R. M. Ramirez, V. S. Bajaj, D. E. Wemmer, A. Pines, M. B. Francis, *Angew. Chem.* **2013**, *125*, 4949 – 4953; *Angew. Chem. Int. Ed.* **2013**, *52*, 4849 – 4853.
[16] M. Kunth, J. Döpfert, C. Witte, F. Rossella, L. Schröder, *Angew. Chem.* **2012**, *124*, 8341 – 8344; *Angew. Chem. Int. Ed.* **2012**, *51*, 8217 – 8220.
[17] J. Sloniec, M. Schnurr, C. Witte, U. Resch-Genger, L. Schröder, A. Hennig, *Chem. Eur. J.* **2013**, *19*, 3110 – 3118.
[18] T. Meldrum, L. Schröder, P. Denger, D. E. Wemmer, A. Pines, *J. Magn. Reson.* **2010**, *205*, 242 – 246.
[19] C. Hilty, T. J. Lowery, D. E. Wemmer, A. Pines, *Angew. Chem.* **2006**, *118*, 76 – 79; *Angew. Chem. Int. Ed.* **2006**, *45*, 70 – 73.
[20] O. Smidsrød, G. Skjåk-Bræk, *Trends Biotechnol.* **1990**, *8*, 71 – 78.
[21] G. K. Seward, Q. Wei, I. J. Dmochowski, *Bioconjugate Chem.* **2008**, *19*, 2129 – 2135.
[22] J. Hennig, A. Nauerth, H. Friedburg, *Magn. Reson. Med.* **1986**, *3*, 823 – 833.
[23] J. Döpfert, C. Witte, M. Kunth, L. Schröder, *Contrast Media Mol. Imaging* **2013**, DOI: 10.1002/cmmi.1543.
[24] L. Schröder, T. Meldrum, M. Smith, T. J. Lowery, D. E. Wemmer, A. Pines, *Phys. Rev. Lett.* **2008**, *100*, 257603.
[25] Q. Wei, G. K. Seward, P. A. Hill, B. Patton, I. E. Dimitrov, N. N. Kuzma, I. J. Dmochowski, *J. Am. Chem. Soc.* **2006**, *128*, 13274 – 13283.
[26] J. M. Chambers, P. A. Hill, J. A. Aaron, Z. Han, D. W. Christianson, N. N. Kuzma, I. J. Dmochowski, *J. Am. Chem. Soc.* **2009**, *131*, 563 – 569.
[27] A. Schlundt, W. Kilian, M. Beyermann, J. Sticht, S. Günther, S. Höpner, K. Falk, O. Roetzschke, L. Mitschang, C. Freund, *Angew. Chem.* **2009**, *121*, 4206 – 4209; *Angew. Chem. Int. Ed.* **2009**, *48*, 4142 – 4145.
[28] G. Duhamel, P. Choquet, E. Grillon, L. Lamalle, J.-L. Leviel, A. Ziegler, A. Constantinesco, *Magn. Reson. Med.* **2001**, *46*, 208 – 212.
[29] B. Driehuys, H. E. Möller, Z. I. Cleveland, J. Pollaro, L. W. Hedlund, *Radiology* **2009**, *252*, 386 – 393.
[30] Z. I. Cleveland, H. E. Möller, L. W. Hedlund, J. C. Nouls, M. S. Freeman, Y. Qi, B. Driehuys, *PLoS ONE* **2012**, *7*, e31306.

